Microgravity Crystallization of Macromolecules: An Interim Report and Proposal for Continued Research

Benjamin E. Goldberg

NASA

Microgravity Crystallization of Macromolecules: An Interim Report and Proposal for Continued Research

Benjamin E. Goldberg

George C. Marshall Space Flight Center
Marshall Space Flight Center, Alabama

ACKNOWLEDGMENTS

PRECEDING PAGE BLANK NOT FILMED

PRECEDING PAGE BLANK NOT FILMED

PAGE _ii_ INTENTIONALLY BLANK

TABLE OF CONTENTS

Page

LIST OF ILLUSTRATIONS

LIST OF TABLES

TECHNICAL PAPER

MICROGRAVITY CRYSTALLIZATION OF MACROMOLECULES: AN INTERIM REPORT AND PROPOSAL FOR CONTINUED RESEARCH

I. INTRODUCTION/BACKGROUND

General

While major resources have been applied and research efforts conducted to exploit crystalline metallic and ceramic materials' advantageous microgravity processing capabilities, little effort has been made for organic, macromolecular or biochemical materials [1-3]. The crystalline polymer systems are not, in general, as dimensionally uniform as non-macromolecular crystals; as such they attenuate transmission of both acoustic and electromagnetic waves to a higher, less desirable degree. As the theoretical capability for molecular engineering of polymer systems is far superior to that of other materials, a need clearly exists for investigation and determination of processing methods designed to promote formation of more ordered crystals.

As solidification from the melt is affected by convective motion, understanding and control of the forces acting on the melt is necessary before improved fabrication techniques can properly be designed [4]. This can be accomplished either by reduction of convection or transformation to a mode in which it is easily controlled. Reduction of buoyancy-driven convection using a low gravity environment may permit production of larger and more nearly perfect crystals. The determination of the viability of a low gravity environment as a preferred processing condition is the goal of this proposed research.

The crystallization process may be divided into two major subprocesses: nucleation and growth. Use of a microgravity environment will permit "containerless" processing that, clearly, will reduce impurity driven heterogeneous nucleation. Far less clear are the effects of gravity reduction on the convective fields in a non-Newtonian liquid, and the subsequent growth of crystals in this type of melt.

The growth process of the macromolecular crystals will be separated from nucleation effects throughout the majority of the recommended research through use of directional solidification techniques. This report details studies dealing qualitatively with the reduction of impurity induced nucleation. With the reduction/elimination of this kinetically controlled process, the effects of gravity on growth may be singled out and quantified, both in-vitro and post-process.

Prior studies by Lovinger and Gryte have centered on attempts to remove random spherulitic structure in favor of unidirectional solidification [5-8]. They processed poly(ethylene oxide) and poly-(propylene) in temperature gradient stage furnaces, minimizing nucleation by translating the sample at speeds $\geq 3\mu m/min$. Thin capillaries have been used by Price and Kilb (PeO) [9], Fujiwara (PP) [10], and Crissman (PE,PP) [11] to minimize nucleation. Stein, et al. unidirectionally crystallized thin films of poly(butene-1) in a thermal gradient [12].

While their research has proven that nucleation is minimized through these processing techniques, little has been determined concerning the effect of thermal gradients and convection on morphology at the growth interface. Lovinger's models do not address these concerns at all. Further, proof of expected nucleation reduction through use of microgravity processing has yet to be demonstrated for polymer systems. The recommended research will center upon characterization of the thermal gradients, both with and without convective forces. These parameters will then be introduced into crystallization models. A thermal gradient stage will be designed and fabricated for this investigation.

Convection

Several types of convective phenomena exist. The two that are affected by gravity are buoyancy-driven convection and surface tension driven (Marangoni) convection. Marangoni flow, while present under all gravitational conditions, generally assumes increased importance as gravity decreases, relative to the effect on buoyancy-driven flow. Qualitatively, a competition between the buoyancy of a hotter (and thereby less dense) component of a homogeneous liquid, and the viscosity of the fluid determines the relative effects of gravity (and coincident convective mixing) of a liquid in a thermal gradient (Fig. 1).

These effects have been quantified for specific configurations. Dimensionless parameters have been defined to characterize liquids, and assess the effects of viscosity and buoyancy [Rayleigh number (Ra)] or surface tension [Marangoni number (Ma)] driven convection [13-16]. The Rayleigh number:

$$Ra = \frac{\alpha \Delta T g d^3}{\kappa \, \nu} \tag{1}$$

where α = volumetric thermal expansion; ΔT is the imposed temperature gradient; g = gravity; d = length of the thermal gradient; κ = thermal conductivity; and ν = viscosity divided by the density (ρ) of the liquid, provides information detailing the critical value for a given configuration at which buoyancy driven convection will occur. Below this value, the relative value of viscosity for the system is high enough to prevent buoyancy driven flow. Similarly, the Marangoni number:

$$Ma = -\frac{\partial \sigma}{\partial T} \frac{\Delta T \, L}{\eta \, \kappa} \tag{2}$$

where $\partial \sigma / \partial T$ = change of surface tension with temperature; and η = viscosity, L = length of the temperature gradient, provides this information for surface tension/viscosity comparisons. The system that will be used for the majority of this research has also been designed to minimize Marangoni flows. Marangoni effects are noted however, in float zone techniques which will be performed to provide ancillary data to this research (Fig. 2) [17].

The critical Rayleigh number for convection in a box (linear theory) has been calculated using models of varying sophistication, and is approximately 2000 [18-19]. Using literature data and preliminary studies for the poly(ethylene) samples to be investigated, all Rayleigh numbers for the highest molecular weight samples are below this critical value. For lower molecular weight samples, the Rayleigh numbers for a normal gravity environment are above this critical value, while those for a microgravity environment (10^{-5} g) are below for the configurations to be investigated [20-22] (see Appendix).

While this justification for the research implies credible existing models for convection, these models are seldom used for correlation to solidification processes [4]. Further, the polymer liquid is non-Newtonian with measured viscosities ranging from 9 x 10^{-5} to 7 x 10^5 Poise [20]. Models have been developed for more ideal liquids. At the critical conditions for convection the shear rate is zero and the higher viscosity values are observed. As the convective flow increases the shear rates increase and lower values of viscosity ensue. The Rayleigh number of the liquid rises accordingly. Planned experiments will track the effect of the convection flows through precise measurement of thermal gradients at the solidification interface. The thermal gradients will be measured through corresponding density variations. The technique of interferometry (or Schleren photography) has been used successfully to document convection phenomenon in simple liquids [23].

The system is further complicated by the shear forces present at the solidification front. The proposed experimental system has been designed to allow translation of the macromolecules, thereby keeping the zone stationary and allowing continuous optical monitoring of the solidification front. This experimental information is necessary for proper modeling and understanding of the non-ideal process of polymer crystallization.

II. COMPLETED STUDIES

Background

Completed studies were centered upon qualitative determination of gravitational effects upon melt-solidified thin films of linear polyethylene. These data encompass, qualitatively and semi-quantitatively, the reduction of heterogeneous nucleation with reduced gravitational forces. Further, characterization data for linear polyethylene has been obtained, allowing calculation of Rayleigh and Marangoni numbers, necessary to assess the feasibility of observing microgravity effects. Finally, a preliminary design for the major experimental apparatus has been prepared, and fabrication is scheduled. Related research, centered upon zone refining of macromolecular systems in reduced gravity environments is also proceeding.

Experimental

Linear polyethylene (M.W. = 48,000, M_w/M_n = 1) was sectioned into 9 micron thick films using a liquid nitrogen cooled microtome. The samples (pellets) were cut from as-cast pellets of unknown thermal history. The cutting temperature was approximately -38°F. The samples were affixed to clean microscope slides. The cleaning procedure involved an initial cleaning with toluene, then acetone, and wiping and drying with dust free laboratory towels. Immediately after cleaning, three zinc chromate dots were placed in equidistant positions on the slide, the sample was centered between the dots and a cover glass (cleaned identically to the slides) was placed, with a 75 ± 10 micron spacing, above. The zinc chromate putty acted as a glue to hold the cover glass position and spacing; DSC and TGA testing indicated no decomposition/deterioration in the thermal region of interest (Figs. 3,4).

The NASA KC-135 aircraft was employed to provide both high (1.8 to 1.9 g's) and micro (0) gravity environments for melt-solidification studies of the polymer films. An experiment cart was designed and fabricated for this portion of the research. All equipment was fastened to this cart, which was in turn bolted to the floor of the aircraft (Fig. 5). The KC-135 makes parabolic arcs which provide microgravity conditions for up to 28 sec.

The cart was designed to allow optical microscopy of the melt-solidification processes. A Mettler hot stage appratus was used; a video tape camera and recorder were also included. An optical photometer, Leitz microscope, an accelerometer and a chart recorder completed the initial cart. The samples were optically monitored during the melt phase transition; these data were later correlated to thermal and gravitational environments. The samples were then air quenched in various gravitational environments; solidification time was experimentally determined to be 15 seconds. All data presented herein are for samples that had a minimum of 20 seconds in a specific gravitational environment during the initial quench period. Finally, the samples were characterized post-flight to determine morphology and subsequently, gravity induced defects.

The characterization effort for the samples consisted of:

1. Correlation of melt kinetics to gravity environment.

2. Correlation of crystallization time to gravity environment.

3. Correlation of sample thickness to crystallization environment.

4. Correlation of optical retardation to crystallization environment.

5. Correlation of relative birefringence to crystallization environment.

6. Correlation of spherulite type to crystallization environment.

7. Correlation of spherulite size to crystallization environment.

8. Correlation of degree of crystallinity to crystallization environment.

The techniques used included:

1. Low angle light scattering (method of Stein [24-25]).

2. Optical microscopy (polarized visual mapping, measuring, Ehringhouse compensator waveplate, depth of focus measurements).

3. Differential scanning calorimetry (Dupont 1090 DSC, method of Mandelkern [26-27]).

4. Fourier transform infrared (Nielsen and Holland [28]).

5. X-ray diffraction (data reduction method of Welcher [29]).

Results

Over one hundred samples were investigated, in both ground and flight tests, to optimize the procedure. Forty-three samples were judged suitable for statistical analysis. The samples were selected based upon the singularity of gravitational environments during both melt and crystallization processes. Any significant variation in gravitation fields during phase transitions disqualified the sample from statistical consideration. The variation in gravitational field was determined through correlation of strip chart data, recorded in-flight, of gravity (uni-axial accelerometer aligned perpendicular to ground), photocell response (mounted on the tri-ocular port of the microscope, provided quantitative data for loss of birefringence during melt/solid transition), and temperature (of the hot stage, from an in-situ thermocouple). Measurements were recorded as a function of time. The removal of the melted samples from the hot stage for the air quench solidification was documented by the photocell response (Fig. 6).

Four major types of accelerational environments were employed in this research: earth normal (1 g, stationary); high gravity (ranging from 1.7 to 1.9 g, non-quantified lateral accelerations); microgravity (ranging from −0.02 to 0.02 g, non-quantified lateral accelerations); and microgravity (ranging from −0.02 to 0.02 g, negligible lateral accelerations). The lateral accelerations were not recorded on the master strip chart for this research, as such this data cannot be correlated for this research. However, other experimenters on the plane did record this information for all three directions; the accelerations

4

were quite low, not rising above the 0.1 g range. The empirical results indicate that, under microgravity conditions, lateral accelerations affect the final morphology. No lateral acceleration correlations are observed under high gravity conditions.

The effects of gravitational accelerations were manifested both macro- and microscopically. Samples recrystallized in a microgravity environment were thicker (48 to 60 microns) than those fabricated in a high gravity environment (20 to 37 microns). Those fabricated in a normal earth environment fell between these extremes (39 to 49 microns). These data were determined through optical focusing, retardation and optical measurement techniques.

Due to the character of the Ehringhouse compensator method, a specific site in the optical field, common to all samples, had to be selected for normalized data gathering. This site corresponded to the cross-hairs of an optical micrometer. The size of the spherulite selected for retardation measurement was also kept approximately constant through careful selection and optical measurement. All data represent the average of at least four readings per sample. Retardation is inversely related to thickness through birefringence, a measure of the microscopic order present in a sample.

White light was used for the retardation measurements, therefore only comparative data — rather than absolute numbers — are presented for the birefringence determinations (Table 1) (see Appendix).

TABLE 1. BIREFRINGENCE

Samples	Number Tested	Comparative Data	Standard Deviation
High gravity	15	1.801	0.006
One gravity	3	1.807	0.006
Zero gravity l.a.	21	1.813	0.007
Zero gravity n.a.	6	1.817	0.005

where zero gravity l.a. = zero gravity with lateral accelerations and zero gravity n.a. = zero gravity with no (free floating) lateral accelerations.

These data indicate that (a) a higher degree of order exists in either the amorphous or crystalline regions of the microgravity samples, or (b) the microgravity samples have a higher percent crystallinity than the higher gravity condition samples. Neither X-ray data, nor DSC data were able to determine a correlation between degree of crystallinity and gravity environment during crystallization.

The X-ray experiments were performed on a Rigaku unit at 32 kV, 20 mA, scan speed of 0.25 deg (two theta)/min from 10 to 30 deg (two theta), with a time constant of 5 sec. A silicon standard was used to calibrate the diffractometer. Samples were mounted on glass fibers with trace amounts of vacuum grease. Because the thin films were only 1 to 2 mm in diameter and variable in shape, the X-ray focussing problems were severe. These problems were addressed by examining the samples in groups of 8, divided according to crystallization gravity (c.g.) conditions (Fig. 7).

The DSC samples were weighed to 0.00001 grams. Sample pans were matched with reference pans to reduce weight effects in experimental error. Although the results for five samples in zero gravity n.a. indicated a degree of crystallization of 91.5 to 93.7 percent, and five high gravity samples displayed numbers from 89.8 to 91.1 percent, the degree of error within the experimental technique makes this

data too close to be statistically significant. No decomposition was noted for any of the samples within the investigated temperature range (20 to 150°C at 10 deg per minute).

As a check on the purity and degree of crystallization of the samples, FTIR investigations were performed. Although slight variations from sample to sample were noted, no clear correlation to c.g. conditions was determined. Only one potential correlatable band was seen; the 1260 cm^{-1} band was more pronounced for the high gravities sample spectra (compared to the peaks at 1352 and 1368 cm^{-1}). One possible explanation for this is a silicone contaminant from the vacuum grease used in the X-ray experiments. This might manifest itself more strongly in the thinner, high gravity samples.

Low angle light scattering was performed to determine the average size of the spherulites present in the samples. Further, this technique allows ranking of the supermolecular ordering, averaged over the beam spot size [24-25]. As several types of supermolecular morphologies were observed microscopically, a normalization methodology had to be developed for the light scattering experiments. For each sample, the best light scattering pattern was photographed, and this was used to determine the spherulite type and size. Sizes were measured using a photodensitometer on the Polaroid negatives; all sample data represents at least four separate data values averaged per sample (Fig. 8).

No significant correlation was found, using this normalization method, between spherulite size and c.g. condition. However, correlation of spherulite type to c.g. conditions were as observed in Table 2.

TABLE 2. LIGHT SCATTERING

Samples	Number of Samples for Spherulite Type		
	a	b	h (poor definition)
High gravity	8	2	4
One gravity	2	1	1
Zero gravity l.a.	13	3	9
Zero gravity n.a.	6	1	

(where a types are the most distinct, h types the least). The regions of the zero gravity – no acceleration – (zero gravity n.a.) crystallization gravity condition samples tested are more distinct; no samples of h type were noted. No such distinctions are seen for the other three gravity conditions.

To eliminate (semi-quantitatively) the biasing that might have been introduced through the normalization technique of the low angle light scattering experiments, optical mapping of each sample was performed. The samples were viewed through crossed polarizers and arbitrarily assigned a value ranging from 1 to 5 based upon the clarity and predominance of the observable degree of supermolecular order. This method was performed at low (40), medium (~400) and high magnifications (~1000X) to characterize adequately the samples. With 1 indicating that the sample appears as a clear spherulitic section, with large, well defined spherulites; and 5 being a sample appearing predominantly amorphous; the results are as given in Table 3 (Fig. 9).

<div align="center">TABLE 3. OPTICAL MICROSCOPY</div>

Samples	Number Tested	Rating	Standard Deviation
High gravity	24	2.82	1.22
Zero gravity l.a.	25	2.52	1.13
Zero gravity n.a.	7	1.64	0.5

This again indicates a difference between the zero gravity n.a. c.g. condition samples and the others. These samples are distinctly more spherulitic, with larger spherulites and less variation, sample to sample. Again each value tabulated is representative of the average of all samples tested, with at least two values per sample counted. Further, these data were compiled by two independent investigators, each rating all samples.

Finally, the orientation of the ordered regions of all samples was investigated. No correlations were noted for the high gravity samples. The remainder of the samples were seen to have a majority of the largest, most distinctive spherulites in regions around the periphery of the slice (Fig. 10). Further investigation revealed that the center portions of these samples were in some contact with the surfaces, both upper and lower, of the glass array. The side regions, which in many cases had become detached from the central portions, were found resting on the lower glass surface or, if still attached, midway between the slide and the cover glass. When the cover glass was removed, the peripheral regions defined above were found to be unattached to the surface, unlike the central portions. The samples crystallized under a high gravity environment were found to rest on the lower, slide surface and had clearly crystallized there.

Discussion

Following the reduction and correlation of the above data, the following scenarios have been developed:

High Gravity Crystallization Conditions:

The surface tension of the molten polymer is insufficient to counteract the effects of the gravitational fields. The samples remain relatively flat and, crystallize on the microscope slide. The slide, though clean, provides numerous sites for heterogeneous nucleation. The samples crystallize non-uniformly, with regions of optically distinct spherulitic ordering (very clean surface regions) and optically poor spherulitic ordering (surface areas providing multiple nucleation sites) (Fig. 11).

Microgravity Crystallization Conditions:

The surface tension effects cause the molten polymer to "ball up;" the post solidification thickness is increased and surface contact with the glass slide is reduced. For some samples slightly negative g-forces lead to contact with the cover glass. Heterogeneous nucleation will again occur most easily in the regions of the sample in contact with the surface. These regions will appear in the central portion of the samples after solidification, the peripheral regions will contain the majority of optically distinct spherulites. Further, the edge sections do not solidify on a surface and are therefore free of the surface post-crystallization, the central regions will again crystallize on the surface. Finally, lateral accelerations will cause additional contact of the polymer to the glass surfaces and provide additional nucleation sites (Fig. 12).

These scenarios are fully compatible with all the data, and explain all but one of the observations. This observation, the birefringence results, requires further discussion and investigation. All the other data has been related to nucleation effects, and subsequent reduction of surface related nucleation in microgravity. The birefringence data, however, indicates a variation in the growth behavior which may correlate with crystallization gravity conditions. This reveals that, while surface nucleation is reduced in microgravity, other significant gravitation related effects are occurring.

The other major effects of gravity reduction are to decrease the buoyancy driven convection and, consequently, increase the relative important of the Marangoni convection effects. For this system, the increase of size of the molten polymer sample (and consequent increase in free surface area) provide for potential Marangoni flow. Further, the thicker sample allows for a higher variation of temperature along the free surface (when compared to higher c.g. condition samples). The samples have surface area perpendicular to the microscope slide (heat sink) for the microgravity case, while in the high gravity case the surface area is more nearly parallel. The resulting difference in Marangoni number may be roughly calculated (Table 4):

TABLE 4. MARANGONI NUMBER VARIATION WITH GRAVITY

	High Gravity	Microgravity
ΔT ($^{\circ}$C)	.2	1–2
L (μm)	28	54
Marangoni Number (percent change)		+1000 to +2000

The Marangoni numbers for the microgravity case are 10 to 20 times those for low gravity: it is these types of data which are necessary to explain the additional gravitational effects.

REFERENCES

1. Pentecost, E. (Compiler): Microgravity Science and Applications Bibliography—1984 Revision. NASA TM 86651, September 1984.

2. Pentecost, E. (Compiler): Materials Processing In Space Bibliography—1983 Revision. NASA TM 82507, January 1983.

3. Pentecost, E. (Compiler): Materials Processing In Space Bibliography. NASA TM 82466, March 1982.

4. Ostrach, S.: J. Fluids Engr., Vol. 105, March 1983, p. 5.

5. Lovinger, A., Chua, J., and Gryte, C.: J. Poly. Sci.: Poly. Phys. Ed., Vol. 15, 1977, p. 641.

6. Lovinger, A. and Gryte, C.: J. Appl. Phys., Vol. 47, No. 5, May 1976, p. 1999.

7. Lovinger, A. and Gryte, C.: Macromol., Vol. 9, No. 2, March-April 1976, p. 247.

8. Lovinger, A., Lau, C., and Gryte, C.: Polymer, Vol. 17, July 1976, p. 581.

9. Price, F. and Kilb, R.: J. Poly. Sci., Vol. 56, 1962, p. 395.

10. Fujiwara, Y.: Kolloid Z.Z. Polym., Vol. 226, 1968, p. 135.

11. Crissman, J. and Passaglia, E.: J. Res. Natl. Bur. Stand., Sec. A, Vol. 70, 1966, p. 225.

12. Sasaguri, K., Yamada, R., and Stein, R.: J. Appl. Phys., Vol. 35, 1964, p. 3188.

13. Chandrasekhar, S.: "Hydrodynamic and Hydromagnetic Stability." Oxford at Clarendon Press, 1961.

14. Lord Rayleigh: Phil. Mag., Vol. 32, 1916, p. 529.

15. Schwabe, D.: Physiochemical Hydrodynamics, Vol. 2, No. 4, 1981, p. 263.

16. Hurle, D. and Jakeman, E., eds.: Physiochemical Hydrodynamics, Vol. 2, No. 4, 1981, p. 237.

17. Goldberg, B.: NASA Internal Memo No. EH34(85-51), July 1985.

18. Davis, S.: J. Fluid Mech., Vol. 30, part 3, 1967, p. 465.

19. Drazin, P.: ZAMP, Vol. 26, 1975, p. 239.

20. Purdue University Ed. Staff, "Thermophysical Properties of Matter — The TPRC Data Series — Thermal Expansion: Nonmetallic Solids," Vol. 13, IFI/Plenum, 1977, p. 1427-1433.

21. Purdue University Ed. Staff, "Thermophysical Properties of Matter — The TPRC Data Series — Thermal Conductivity: Nonmetallic Solids," IFI/Plenum, 1977, p. 956.

22. Gaines, G., Jr.: Polym., Eng. Sci., Vol. 12, 1972, p. 1.

23. Howes, W.: Appl. Optics, Vol. 23, No. 10, 1984, p. 1467.

24. Prud'homme, R., Yoon, D., and Stein, R.: J. Poly. Sci.: Poly. Phys. Ed., Vol. 11, 1973, p. 1047.

25. Mandelkern, L., Go, S., Peiffer, D., and Stein, R.: J. Poly. Sci.: Poly. Phys. Ed., Vol. 15, 1977, p. 1189.

26. Mandelkern, L., Fatou, J., Denison, R., and Justin, J.: Polymer Letters, Vol. 3, 1965, p. 803.

27. Mandelkern, L., Allou, A., Jr., and Gopalan, M.: J. of Phys. Chem., Vol. 72, No. 1, 1968, p. 309.

28. Nielsen, J. and Holland, R.: J. Molecular Spec., Vol. 6, 1961, p. 394.

29. Welcher, F.: Standard Methods of Chemical Analysis, Vol. 3, 1964, p. 1583.

APPENDIX

Values for Calculations:

Thermal expansion = α = 0.001/°K

Temperature gradient = ΔT = 25°K

Gravity = g = 980 cm/sec^2

Gradient length = d = 0.65 cm

Thermal conductivity = κ = 6 x 10^{-4} cal/cm s°K

Viscosity = η = 1 dyne sec/cm^2

Specific heat = C_p = 0.53 cal/gm°K

density = ρ = 0.90 gm/cm^3

$$\frac{d\sigma}{dT} = -0.06 \text{ dyne/cm°K}$$

Rayleigh Number Calculation:

$$\kappa/\rho\,C_p = \frac{(6 \times 10^{-4} \text{ cal/cm s°K})}{(0.53 \text{ cal/gm°K})(0.90 \text{ gm/cm}^3)} = 0.001 \text{ cm}^2/s$$

$$\nu = \eta/\rho = \frac{(1 \text{ dyne sec/cm}^2)}{(0.90 \text{ gm/cm}^3)} = 1.1 \text{ cm}^2/s$$

$$Ra = \frac{\alpha\,\Delta Tgd^3}{\kappa\,\nu} = \frac{(0.001/°K)(25°K)(980 \text{ cm/s}^2)(0.65 \text{ cm})^3}{(0.001 \text{ cm}^2/s)(1.1 \text{ cm}^2/s)} = 6117$$

Marangoni Number Calculation:

gradient length = L = 0.25 cm

$$Ma = \frac{-d\sigma}{dT}\frac{\Delta T\,L}{\eta\,\kappa} = \frac{(0.06 \text{ gm cm/sec}^2 \text{ cm°K})(5°K)(0.25 \text{ cm})}{(1 \text{ dyne sec/cm}^2)(0.001 \text{ cm}^2/s)} = 75$$

Birefringence Calculation:

Γ = retardation

F = 2i = 2 x (reading in θ from Ehringhouse compensator)

C = correction factor for incident wavelength = 4.787 for polychromatic light

$\log\Gamma = \log F + \log C$
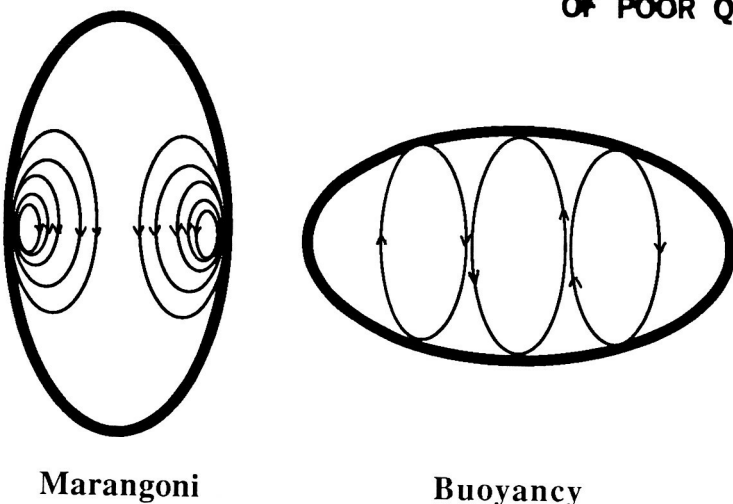
Marangoni   **Buoyancy**

Figure 1. Marangoni versus buoyancy driven convection.
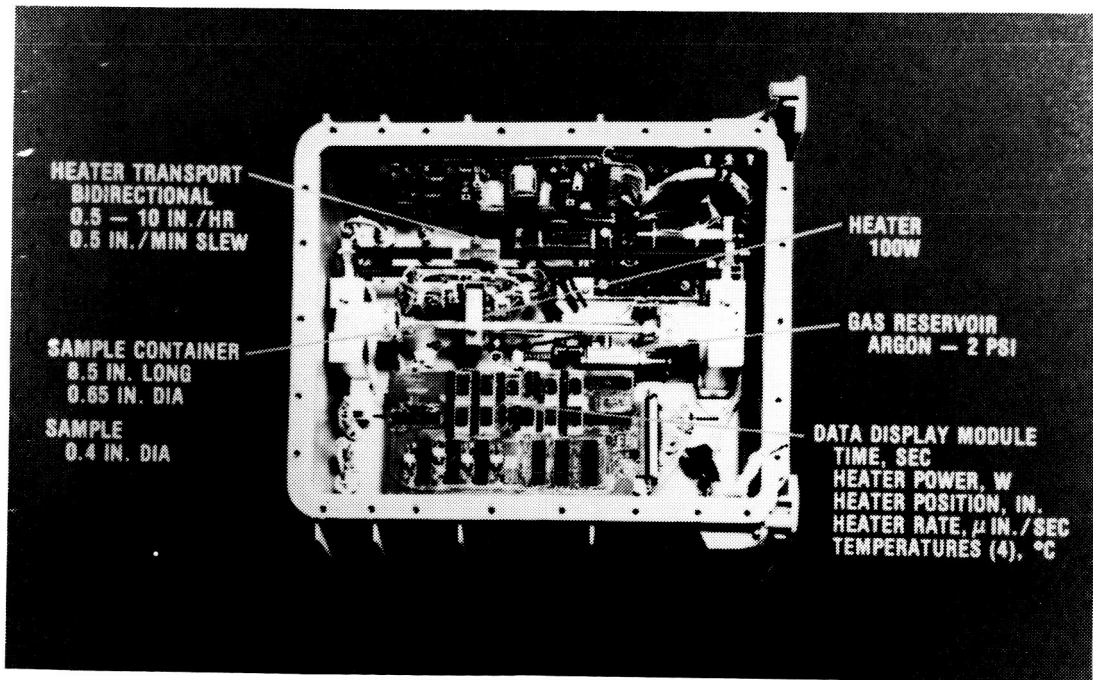
The Rockwell hardware, initially constructed for a student flight experiment, is being modified for low temperature, macromolecular float zone experiments. This work may provide additional information for the proposed dissertation research.

Figure 2. Microgravity float zone apparatus.

Top View

☐ microscope slide   ▦ cover glass

▦ zinc chromate putty   ☒ poly(ethylene)

↕ 75 microns

Side View
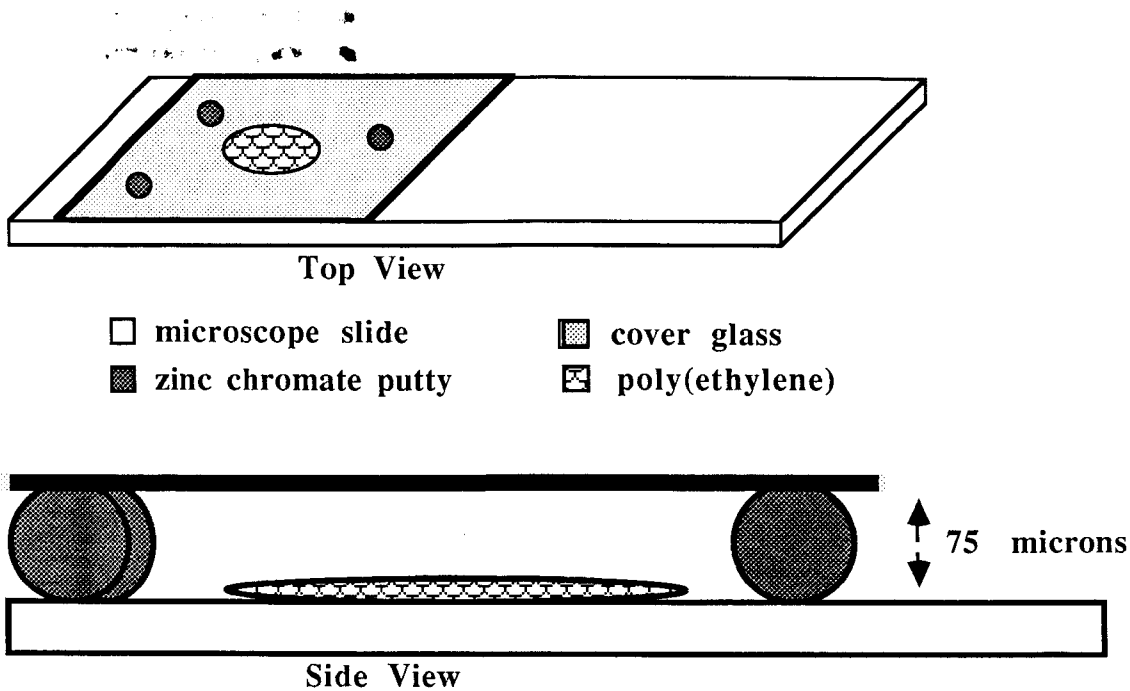
Figure 3. Sample configuration.

Sample: PE 67
Size: TINY
Rate: 10 DEG/MIN
Program: Interactive DSC V3.0

DSC

Date: 2-Aug-85 Time: 12:56:39
File: PUTTY.04 CLB DATA CORP
Operator: GOLDBERG
Plotted: 2-Aug-85   13:25:47

Polyethylene

Zinc Chromate

Heat Flow (mW)

Temperature (°C)

DuPont 1090
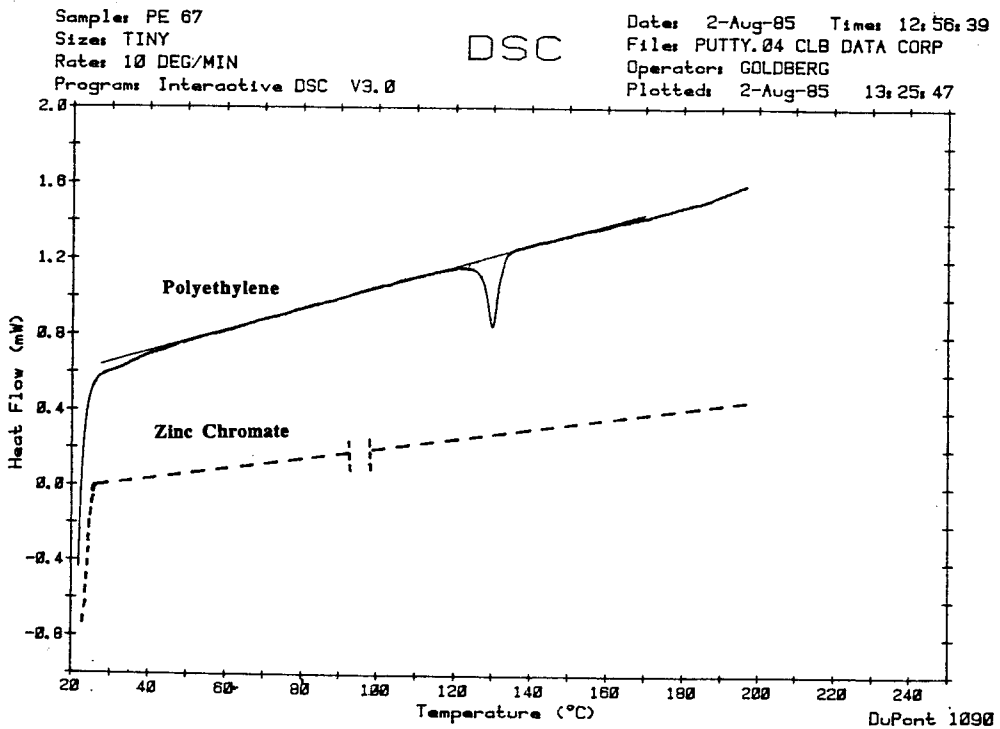
No significant transitions are noted for the zinc chromate putty. The melt transition for poly(ethylene) occurs at 127-132 degrees C. (heating rate 10 deg. C/min.)

Figure 4. Differential scanning calorimetry traces.

Pictured: B. Goldberg and B. Shurney exchanging samples during microgravity period. Cart must be left untouched during melt cycle to prevent lateral accelerations.

Figure 5. Flight cart configuration for microgravity crystallization/nucleation studies.
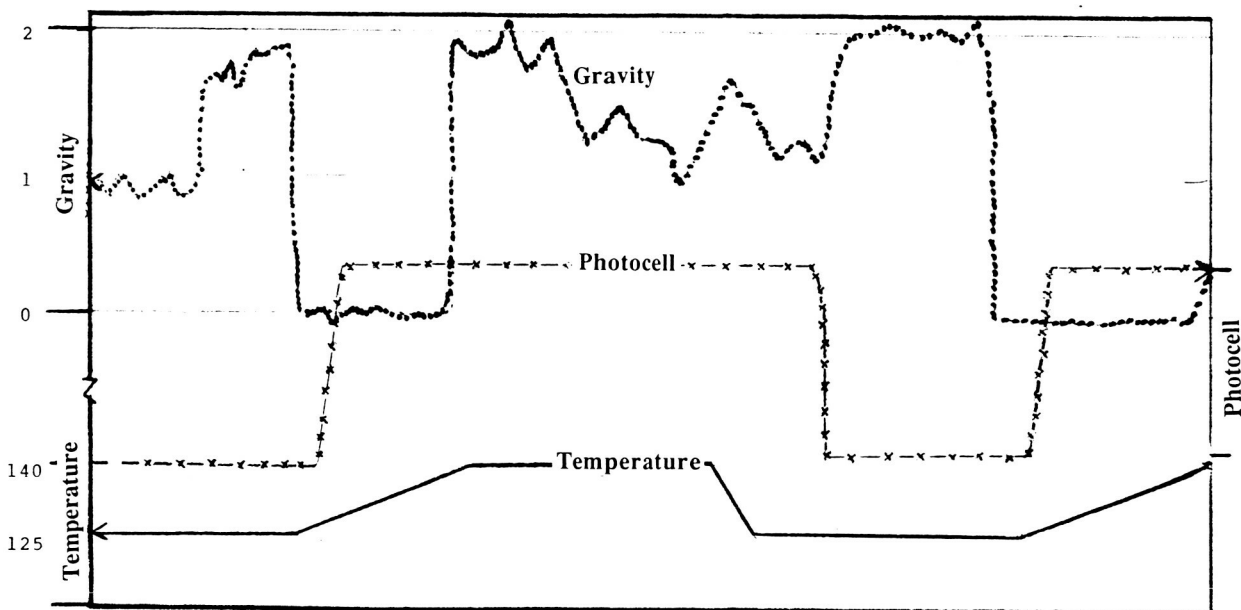
These traces have been smoothed and offset to correct for instabilities and pen locations on actual record.

Figure 6. Idealized strip chart record of KC-135 flight experiment.

15
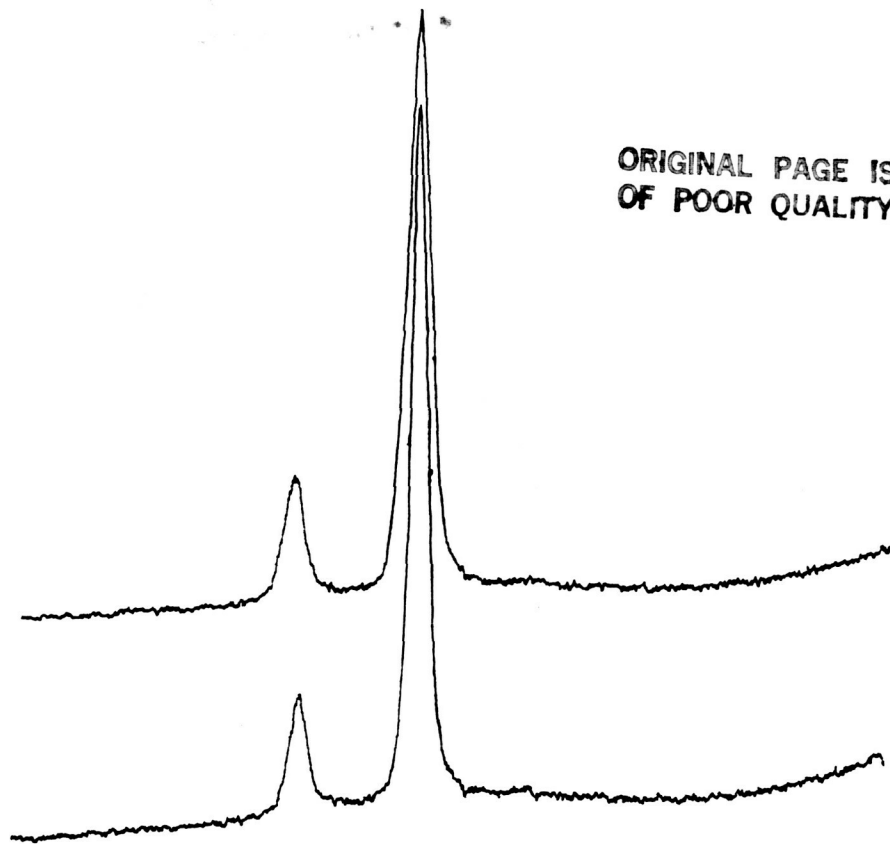
X-ray traces, presented for high and low gravity environment samples display no significant variations. Each trace represents an average over eight samples.

Figure 7. X-ray traces.

(a)   (h)
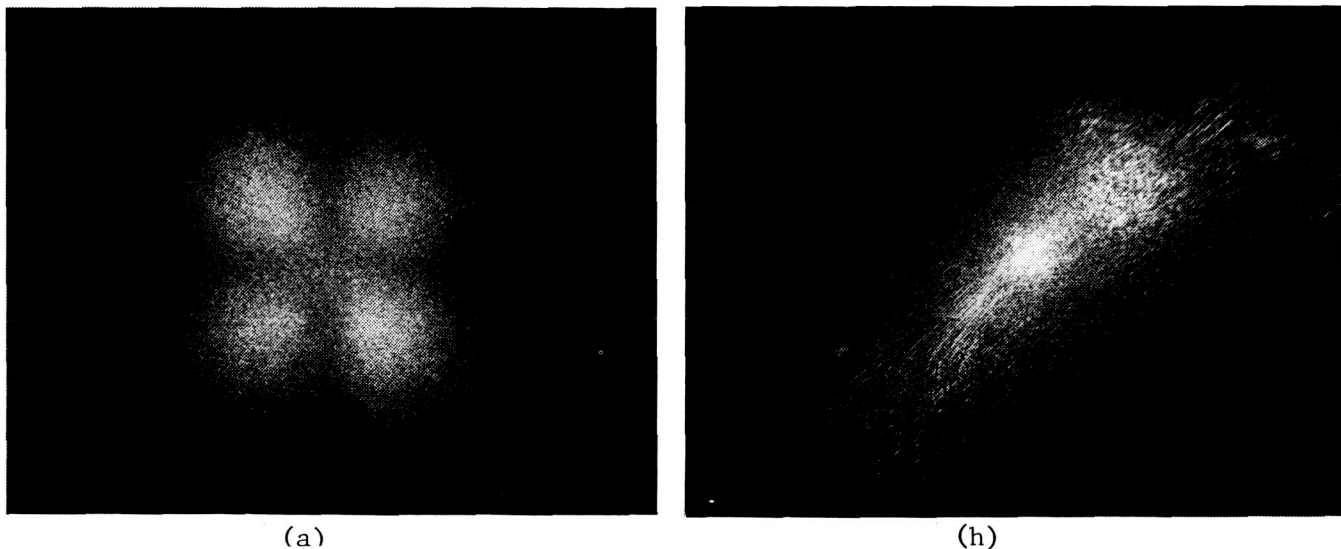
The images denoted as (a) and (h) are distinctly different. Measurements of highest intensity for each figure were made with an optical photo-densitometer.

Figure 8. Representative light scattering images.

a

b
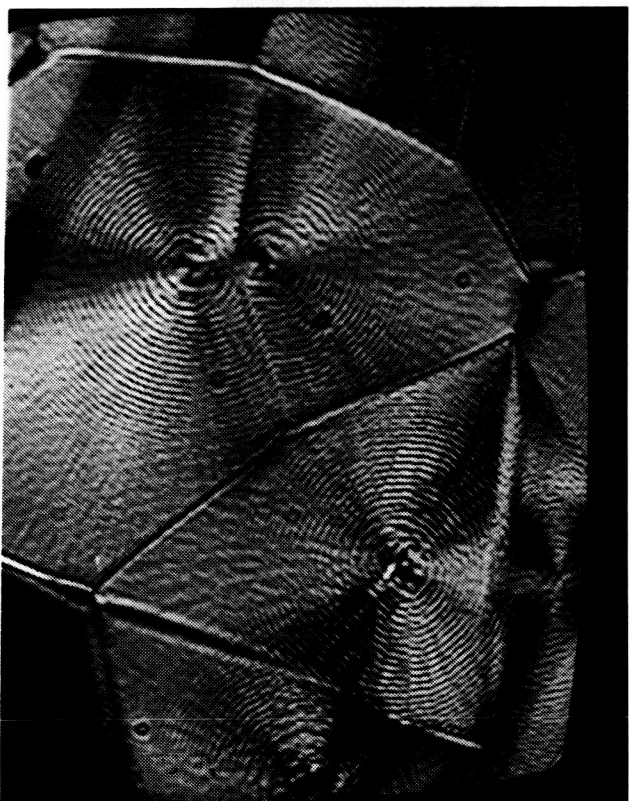
c

a) rough surface, non-distinct spherulites, many nucleation sites. (Magnification 600 X)
b) More clearly defined spher-ulites; fewer nucleation sites. (Magnification 600 X)
c) Large, distinct spherulites, few nucleation sites. (Magnification 600 X)

Figure 9. Morphology types.
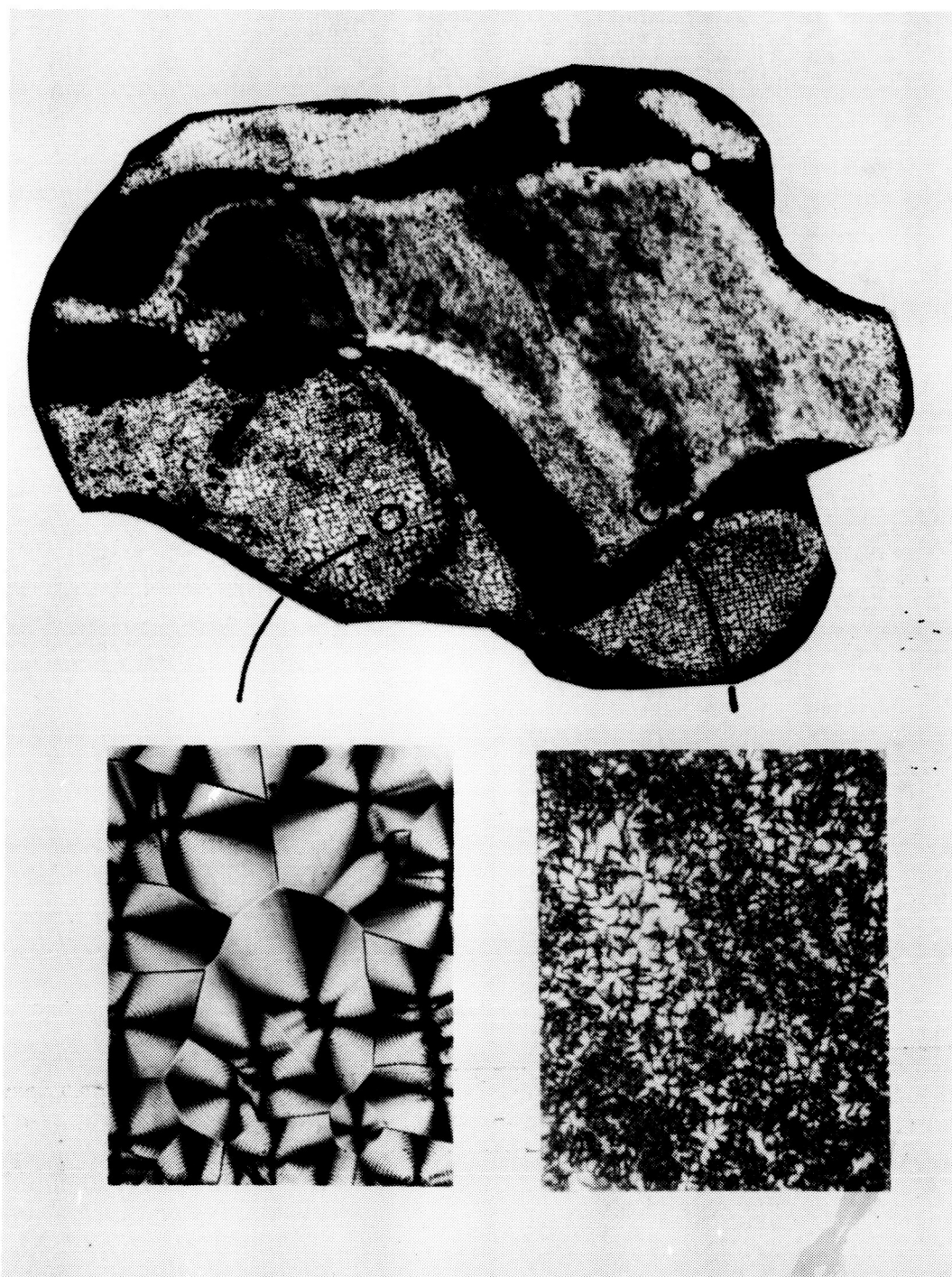
While several, distinct optical morphologies are present in one sample, the trend for the regions of distinct spherulitic ordering is toward the edges of the sample. The blown up regions (330 X), taken from the sites noted on the sample (30 X) are representative for microgravity (no acceleration) processed samples. (See Figure 12)

Figure 10. Photographic montage of an entire sample.

Initial state of sample.

poorly defined spherulites
distinct spherulites
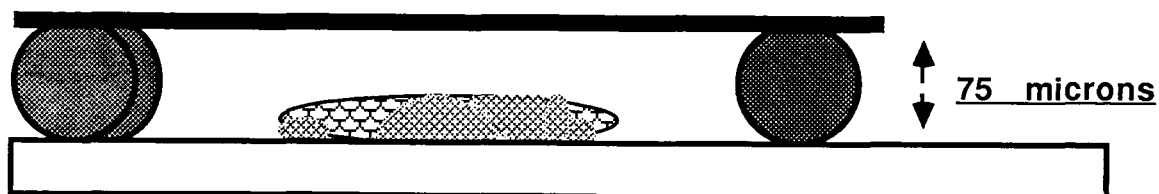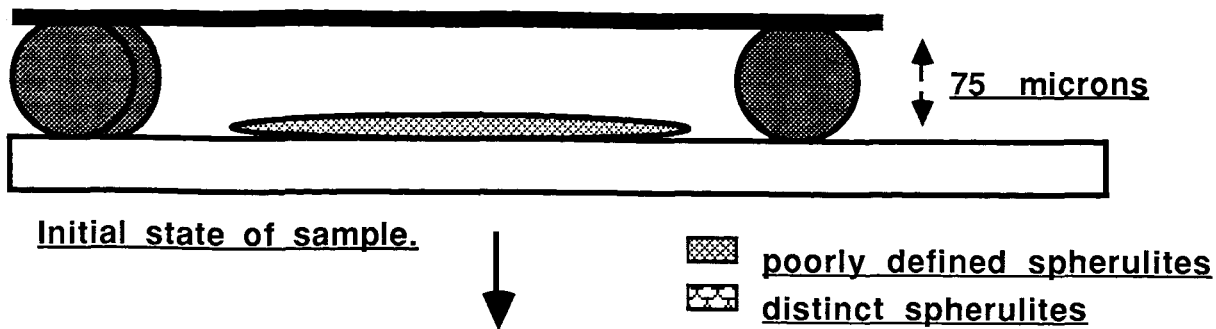
After melt and recrystallization. Sample's surface tension cannot fully counteract gravitation forces; large surface area provides nucleation sites.

Figure 11. High gravity scenario.

Initial state.
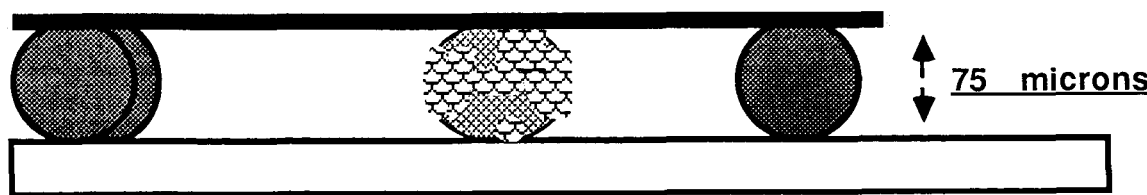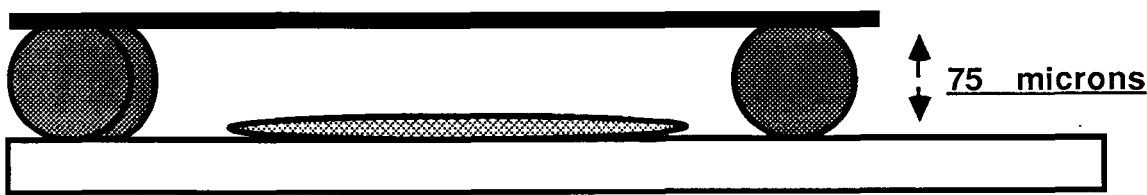
Recrystallizing molten polymer system under microgravity. Note large free surface area.
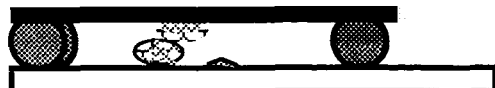
Lateral accelerations cause additional surface contact.

No accelerations: sample solidifies with minimum contact.

Figure 12. Microgravity scenario.

19

1. REPORT NO. NASA TP-2671	2. GOVERNMENT ACCESSION NO.	3. RECIPIENT'S CATALOG NO.
4. TITLE AND SUBTITLE Microgravity Crystallization of Macromolecules: An Interim Report and Proposal for Continued Research		5. REPORT DATE DECEMBER 1986
		6. PERFORMING ORGANIZATION CODE
7. AUTHOR(S) Benjamin E. Goldberg		8. PERFORMING ORGANIZATION REPORT #
9. PERFORMING ORGANIZATION NAME AND ADDRESS George C. Marshall Space Flight Center Marshall Space Flight Center, Alabama 35812		10. WORK UNIT NO. M-543
		11. CONTRACT OR GRANT NO.
12. SPONSORING AGENCY NAME AND ADDRESS National Aeronautics and Space Administration Washington, D.C. 20546		13. TYPE OF REPORT & PERIOD COVERED Technical Paper
		14. SPONSORING AGENCY CODE

15. SUPPLEMENTARY NOTES
Prepared by Materials and Processes Laboratory, Science and Engineering Directorate.

16. ABSTRACT

An initial investigation exploring the effects of gravity on the crystallization of macromolecular systems has been completed. Monodisperse poly(ethylene), molecular weight 48,000 was melted and recrystallized under three gravitational conditions: 0, 1, and 2 g. No correlations to gravitational environment were noted for the 20°C/min melt, as monitored with a photodensitometer system. However, post-crystallization testing of the recrystallized samples revealed thicker samples with more regions of large, well defined spherulites for the zero gravity crystallization environment.

The results of the post-crystallization analysis have been reviewed and the results related to nucleation concerns. Finally, birefringence data, consistent with, but not explained by, the nucleation scenarios is detailed, and further investigations are proposed.

17. KEY WORDS Microgravity Polymers Crystallization Nucleation Convection	18. DISTRIBUTION STATEMENT Unclassified – Unlimited Subject Category 27

19. SECURITY CLASSIF. (of this report) Unclassified	20. SECURITY CLASSIF. (of this page) Unclassified	21. NO. OF PAGES 24	22. PRICE A02